Quantum Interference Spectroscopy of Rubidium-Helium Exciplexes Formed on Helium Nanodroplets

M. Mudrich* and F. Stienkemeier
Physikalisches Institut, Universität Freiburg, 79104 Freiburg, Germany

G. Droppelmann and P. Claas
Fakultät für Physik, Universität Bielefeld, 33615 Bielefeld, Germany

C. P. Schulz
Max-Born-Institut, Max-Born-Straße 2a, 12489 Berlin, Germany
(Received 3 September 2007; published 15 January 2008)

Femtosecond multiphoton pump-probe photoionization is applied to helium nanodroplets doped with rubidium (Rb). The yield of Rb^+ ions features pronounced quantum interference (QI) fringes demonstrating the coherence of a superposition of electronic states on a time scale of tens of picoseconds. Furthermore, we observe QI in the yield of formed RbHe exciplex molecules. The quantum interferogram allows us to determine the vibrational structure of these unstable molecules. From a sliced Fourier analysis one cannot only extract the population dynamics of vibrational states but also follow their energetic evolution during the RbHe formation.

DOI: 10.1103/PhysRevLett.100.023401 PACS numbers: 36.40.−c, 31.70.Hq, 37.10.Jk

One of the great achievements of femtosecond (fs) lasers has been the observation in real time of the formation and breaking of chemical bonds between two atoms [1]. The molecular dynamics is visualized when initializing a nonstationary multistate superposition (wave packet, WP) by a fs pump pulse, by letting the WP evolve freely in time, and by projecting it onto a final state by the second probe pulse [pump-probe (PP) technique]. This final state is subsequently detected with time-independent methods, e.g., by measuring the spontaneous fluorescence or the yield of photoions.

A different approach to molecular WP dynamics is WP interferometry based on excitation by two identical fs pulses with a well-defined relative phase in an interferometric setup. This approach relies on the interference of WP amplitudes excited according to two temporally distinct quantum paths leading to the same final state [2]. In the limit of weak fields this approach is equivalent to quantum beats, Ramsey fringes in the time domain [3,4], Fourier spectroscopy using fs pulses [5], or temporal coherent control [6]. The measured quantum interferograms carry the high-frequency oscillation of the electronic energy modulated by the low-frequency beatings of WP motion.

Direct measurement of QI oscillations allowed us to study the dynamics of atomic Rydberg states, electronic spin and nuclear spin WPs of free atoms in the gas phase [3–8], of atoms on surfaces [9], and of atoms attached to helium nanodroplets [10]. Different variants of WP interferometry have also been applied to simple molecules [11–15] and even to molecular crystals [16]. Using pump-probe spectroscopy with phase-locked pulses the dynamics of electronic as well as vibrational coherence of Cl_2 molecules embedded in solid Ar has been investigated [15]. As a recent highlight, high-precision WP interferometry with HgAr and I_2 dimers has been demonstrated allowing to prepare arbitrary relative populations in different vibrational states [14].

Helium nanodroplets are widely applied as a nearly ideal cryogenic matrix for spectroscopy of embedded molecules and as nanoscopic reactors for studying chemical reactions at extremely low temperatures [17–19]. Only recently, the real-time dynamics of doped helium nanodroplets have been studied in pump-probe experiments [20]. Alkali atoms and molecules represent a peculiar class of dopant particles due to their extremely weak binding to the surface of helium nanodroplets. Thus they can be viewed as intermediate systems between the gas phase and conventional cryogenic matrices.

In this Letter, we report on QI spectroscopy upon excitation of Rb atoms attached to helium nanodroplets. In particular, we interpret interference structures in RbHe exciplex molecules which are formed upon excitation of Rb into the $5p$ state, demonstrating that coherence even survives the formation of a chemical bond. The quantum interferogram is analyzed to extract the vibrational spectrum of the unstable RbHe molecule by Fourier transformation.

In the experiment, a fs laser system is combined with a helium nanodroplet molecular beam machine. The experimental setup is identical to the one used in former experiments [21]. Superfluid helium nanodroplets are formed in a supersonic expansion of helium gas at a high stagnation pressure (50×10^5 Pa) from a cryogenic nozzle ($T = 19$ K). The generated droplets have a mean droplet size of 10 nm and cool by natural evaporation to a terminal

temperature of 380 mK which is well below the transition temperature to superfluidity. The droplets are doped with single alkali atoms which are picked up in a heated vapor cell further downstream. The weak interaction of alkali atoms with helium leads to so called "bubbles" where the solvation environment is characterized by a diminished helium density. In helium droplets alkalis therefore reside in surface states; i.e., the atoms are weakly bound on top of dimplelike textures [22]. Because binding energies are only around 10 K, which is small compared to energies of laser-induced processes, desorption from the droplets dominantly follows laser excitations.

Pairs of fs laser pulses with ≈110 fs pulse duration and equal intensity are generated by a Mach-Zehnder interferometer and propagate collinearly with variable delay time up to 100 ps with a step increment down to 220 attoseconds. In the probe step Rb^+ and $RbHe^+$ photoions are formed which are subsequently detected mass selectively in a quadrupole mass spectrometer.

Note that Rb atoms are excited on the helium droplets but are detected either as free atoms or as free RbHe exciplexes after having left the droplet. The photoionization signals detected on the mass of bare Rb^+ ions (85 amu) and on the mass of $RbHe^+$ ions (89 amu) as a function of delay time between pump and probe pulse are depicted in Figs. 1(a) and 1(b), respectively. In (a), the laser

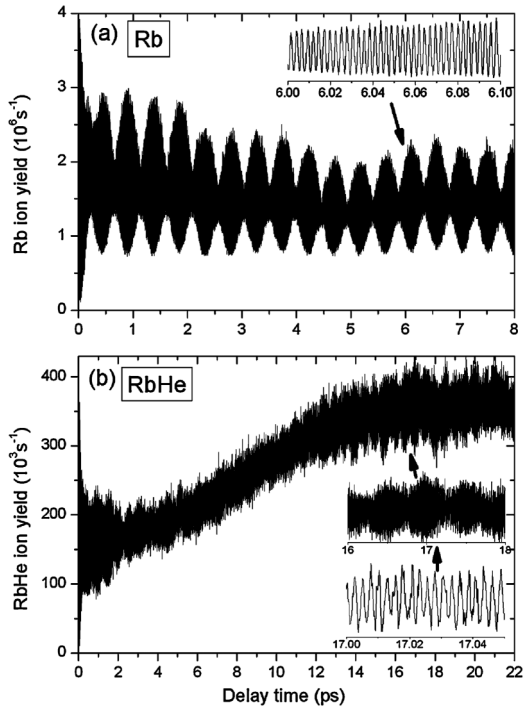

FIG. 1. (a) Yield of photoionized Rb atoms excited on the surface of helium nanodroplets as a function of the delay between femtosecond pump and probe pulses. The inset shows that by choosing a step increment of 220 attoseconds the QI oscillation is fully resolved. (b) QI fringes of ionized RbHe exciplexes detected on mass 89 amu. The amplitude modulation comprehends the vibrational structure of the RbHe molecule.

wavelength is tuned to $\lambda = 775$ nm which leads to a Σ-type excitation with purely repulsive interaction between the excited p-orbital of Rb and the He surface. In this case the Rb atoms rapidly desorb from the He droplets. Consequently, the influence of the helium environment does not play a role when probing free Rb atoms after long delay times.

The ion yield is strongly modulated by QI oscillations. The fast oscillation, corresponding to the excitation frequency with a period of about 2.6 fs [inset of Fig. 1(a)], clearly displays a beat note with a period of 0.47 ps. In addition, half a period of a 11 ps-beat note is recognizable from the slow drop of oscillation amplitude from $t = 0$ until $t \approx 5$ ps. These beat frequencies are readily interpreted by energy differences between levels which are coherently excited in the PP scheme, as illustrated in Fig. 2(a). Coincidentally, the $5p_{3/2} \leftarrow 5s$ (E_1 in Fig. 2) and the $5d_{3/2}(5d_{5/2}) \leftarrow 5p_{3/2}$ (E_2 in Fig. 2) transitions are energetically different only by $\Delta E = E_2 - E_1 = 67.44(70.40)$ cm^{-1}, which is less than the spectral width of the laser pulse (140 cm^{-1}). Thus the two levels $5p$ and $5d$ can be coherently excited by the pump pulse which causes the 0.47 ps-beat pattern. The slow 11 ps beat results from the 2.96 cm^{-1} fine structure splitting between $5d_{3/2}$ and $5d_{5/2}$ states. On the other hand, the $J = 1/2$ fine structure component of the $5p$ state is separated from the $J = 3/2$ state by 237.6 cm^{-1} and does not contribute to the spectra shown here.

At certain excitation wavelengths, where the alignment of the excited p-orbital is parallel to the surface of the droplet, the attractive interaction of this configuration leads to the formation of RbHe exciplex molecules [21]. The maximum yield of RbHe exciplexes is obtained when

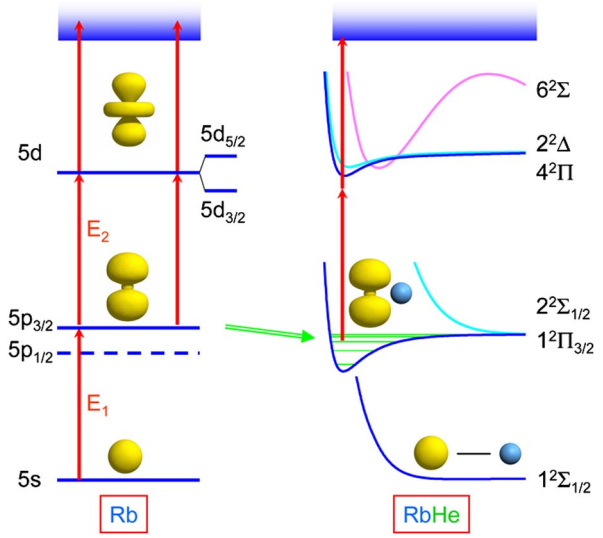

FIG. 2 (color online). Pump-probe excitation schemes showing the involved electronic states of Rb atoms (left side) as well as the vibronic states after having formed a RbHe exciplex [23]. The spatial distributions of the electron orbitals in corresponding states are also sketched.

tuning the fs laser to $\lambda = 780$ nm. In previous PP experiments the formation time of RbHe exciplexes has been measured to $\tau \approx 8$ ps [21]. Accordingly, the $RbHe^+$ ion yield depicted in Fig. 1(b) increases continuously from $t = 0$ to $t = 15$ ps. The initial signal level of about 45% of the maximum signal is due to ionization of RbHe molecules which have been excited by previous laser pulse pairs of the fs pulse train. Besides the exciplex formation dynamics, the PP transients recorded on the RbHe mass feature QI fringes as well [21]. Hence, coherence of the electronic superposition state excited by the pump pulse in Rb atoms appears to be conserved upon binding of a He atom to the Rb. The amplitude of the RbHe QI also shows a well-defined modulation pattern. However, at first sight no obvious beat frequencies can be identified, suggesting that a variety of frequency components contribute to the beat signal.

In this Letter, the interference fringes are quantitatively analyzed for extracting information about the coherently excited energy levels. To this end, the PP transients of Fig. 1 are Fourier transformed in the entire delay time range. The Fourier spectra of the envelope function of the interference oscillations are shown in Fig. 3(a). As expected, the Rb spectrum features only one frequency component corresponding to the energy difference $E_2 - E_1$. The observed value 70.4(3) cm^{-1} matches the value for the $5d_{5/2} \leftarrow 5p_{3/2}$ transition, due to the larger transition moment to the $5d_{5/2}$ state compared with the $5d_{3/2}$ state.

The RbHe spectrum contains 4 distinct maxima at frequencies 8.8(6) cm^{-1}, 23.2(7) cm^{-1}, 43.7(2) cm^{-1}, and at 65.8(3) cm^{-1}. These frequencies can be attributed to the energy differences between neighboring vibrational levels of the RbHe molecule. Because of the unstable nature of the molecule, these have not been determined experimentally before. Therefore only theoretical predictions are available for comparison. We constructed a Morse potential from a linear fit of the measured level spacings. The fit result is included in Fig. 3 as a comb representation. The corresponding Morse potential is depicted by the solid line in Fig. 3(b). For comparison, the *ab initio* potential of Pascale [23] is plotted in the same diagram as a dashed line. The position of the minimum of the Morse potential is set to coincide with the one of the *ab initio* potential. The well depths of the Morse and the *ab initio* potentials (-180.9 cm^{-1} and -133.9 cm^{-1}, respectively) deviate by 25%, which is reasonable agreement in view of the limited accuracy of the *ab initio* calculations and the simple model potential used to fit the data.

The relative heights of measured peaks indicate that all vibrational levels are populated with similar probabilities. This goes perfectly along with observations of emission spectra in KHe exciplexes for which the populations of vibrational states were quantified [24]: Depending on the excitation laser frequency, slightly more pronounced lower or higher vibrational states, respectively, have been observed in this very similar system. In our experiment we can also tune the population of vibrational levels by varying the femtosecond laser frequency or pulse characteristics.

More importantly, it is shown that our real-time approach not only unravels the vibrational energy structure of the unstable RbHe molecule but that we can even follow the evolution of the vibrational structure during the formation process of the molecule. The time dependence of the frequency components can be visualized by Fourier transforming the data inside a time window of fixed length (2 ps) which slides across the entire scan range. The resulting spectrogram of RbHe is depicted in Fig. 4 as a contour plot. The individual frequency components discussed before appear as vertical lines in the upper half of the spectrogram at delay times $t \geq 12$ ps, meaning that energies do not change with time. In contrast to that, at short delay times (<10 ps) one can observe shifts. These are not very pronounced in the data set presented in this Letter but are clearly present when using different excitation wavelengths (not shown in this Letter). The shifts are of the order 10 cm^{-1}, which nicely correlates with the binding energy of RbHe to the droplet prior to desorption.

In the formation process the molecules are formed near the dissociation limit and then vibrationally cool through the interaction with the helium droplet before they desorb and subsequently keep their population [24]. This cooling mechanism can also be followed in the spectrogram: At delay times shorter than 4 ps there is much more intensity at lower frequencies which represent energy differences between higher lying levels. At longer times, intensity distributes almost equally over all the lines. By changing

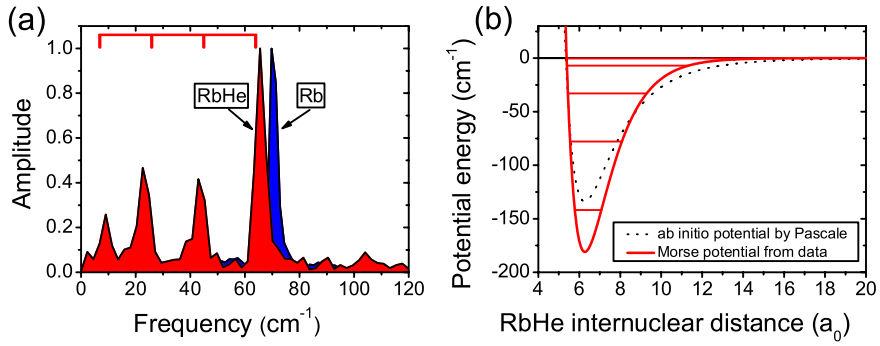

FIG. 3 (color online). (a) Fourier transforms of the amplitude functions of the quantum interferograms of the Rb and RbHe data shown in Fig. 1. The spectrum of Rb is dominated by the frequency component $E_2 - E_1$, whereas the RbHe spectrum displays a vibrational progression. (b) Morse potential reconstructed from a fit of the vibrational spectrum in comparison with an *ab initio* potential [23].

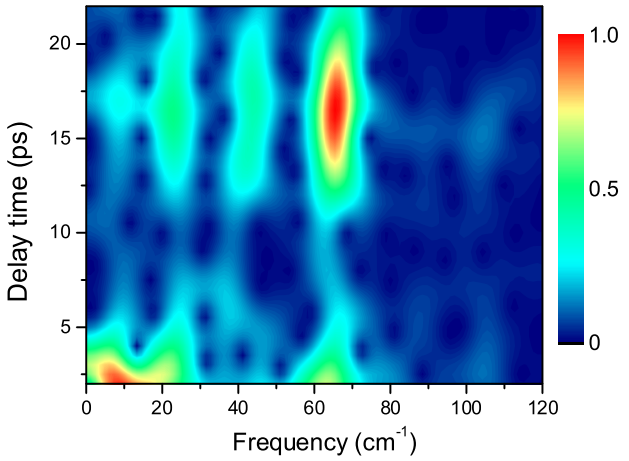

FIG. 4 (color online). Spectrogram of the RbHe QI oscillation showing the time evolution of the energy and the population of the coherently excited states.

the excitation laser wavelength by a few nm, the relative amplitudes of the individual lines can be slightly changed.

Finally, the issue of decoherence has to be discussed. It is striking that during the observed range of delay times (20 ps) the amplitude of the interference fringes does not decrease at all, although initially the phase information is put into the excitation of the very weakly bound Rb atoms on the droplets and the oscillation is observed in the yield of RbHe molecules which have formed and detached from the droplet. As discussed by Shapiro [25], in dissociation reactions coherence of the fragments is maintained in the case of broadband laser excitation. The same arguments can be applied to association of RbHe molecules. However, cooling of vibrational excitations of the RbHe molecule by dissipation of energy into the helium droplet must be allowed for as a source of decoherence. Indeed, in the case of KHe exciplex formation, a fast decay of the QI contrast within 1.5 ps is observed [10]. Thus, the dynamics of decoherence in these systems that are weakly coupled to helium nanodroplets appears to sensitively depend on the internal structure and on the coupling strength to the helium environment. This will be studied more systematically in future experiments. The result of our experiments that electronic coherence survives the formation and cooling process without severe suppression is a valuable piece of information, demonstrating that coherent control techniques are not impeded by the formation or breaking of bonds. In comparison with large, e.g., biological molecular complexes, our system is, of course, a clean and well-defined process which relies on such low temperatures.

In conclusion, we have demonstrated that QI structures can be used not only to determine binding properties of small molecules but also to characterize the reaction process in real time. Changes in the vibrational structure as well as changes in their population can be directly monitored. More importantly, the bond formation process does not destroy coherent properties showing that this kind of coherent control experiments can in principle be applied to more complex systems.

Stimulating discussion with M. Shapiro, B. Girard, and T. Baumert and financial support by the Deutsche Forschungsgemeinschaft are gratefully acknowledged.

*mudrich@physik.uni-freiburg.de

[1] A. Zewail, *Femtochemistry—Ultrafast Dynamics of the Chemical Bond* (World Scientific, Singapore, 1994).
[2] P. W. Brumer and M. Shapiro, *Principles of the Quantum Control of Molecular Processes* (Wiley-VCH, Berlin, 2003).
[3] L. D. Noordam, D. I. Duncan, and T. F. Gallagher, Phys. Rev. A **45**, 4734 (1992).
[4] J. F. Christian, B. Broers, J. H. Hoogenraad, W. J. van der Zande, and L. D. Noordam, Opt. Commun. **103**, 79 (1993).
[5] M. Bellini, A. Bartoli, and T. W. Hänsch, Opt. Lett. **22**, 540 (1997).
[6] V. Blanchet, C. Nicole, M.-A. Bouchene, and B. Girard, Phys. Rev. Lett. **78**, 2716 (1997).
[7] R. R. Jones, Phys. Rev. Lett. **75**, 1491 (1995).
[8] A. Präkelt, M. Wollenhaupt, C. Sarpe-Tudoran, and T. Baumert, Phys. Rev. A **70**, 063407 (2004).
[9] S. Ogawa, H. Nagano, and H. Petek, Phys. Rev. Lett. **82**, 1931 (1999).
[10] F. Stienkemeier *et al.*, Phys. Rev. Lett. **83**, 2320 (1999).
[11] N. F. Scherer *et al.*, J. Chem. Phys. **95**, 1487 (1991).
[12] V. Blanchet, M. A. Bouchene, and B. Girard, J. Chem. Phys. **108**, 4862 (1998).
[13] C. Warmuth *et al.*, J. Chem. Phys. **112**, 5060 (2000).
[14] K. Ohmori, Y. Sato, E. E. Nikitin, and S. A. Rice, Phys. Rev. Lett. **91**, 243003 (2003); K. Ohmori *et al.*, *ibid.* **96**, 093002 (2006).
[15] M. Fushitani, M. Bargheer, M. Gühr, and N. Schwentner, Phys. Chem. Chem. Phys. **7**, 3143 (2005).
[16] A. Tortschanoff, K. Brunner, C. Warmuth, and H. F. Kauffmann, J. Chem. Phys. **110**, 4493 (1999).
[17] F. Stienkemeier and A. F. Vilesov, J. Chem. Phys. **115**, 10 119 (2001).
[18] J. P. Toennies and A. F. Vilesov, Angew. Chem. **43**, 2622 (2004).
[19] E. Lugovoj, J. P. Toennies, and A. F. Vilesov, J. Chem. Phys. **112**, 8217 (2000).
[20] F. Stienkemeier and K. Lehmann, J. Phys. B **39**, R127 (2006); P. Claas *et al.*, J. Phys. Chem. A **111**, 7537 (2007); P. Claas *et al.*, J. Phys. B **39**, S1151 (2006).
[21] G. Droppelmann, O. Bünermann, C. P. Schulz, and F. Stienkemeier, Phys. Rev. Lett. **93**, 023402 (2004).
[22] F. Stienkemeier, O. Bünermann, R. Mayol, F. Ancilotto, M. Barranco, and M. Pi, Phys. Rev. B **70**, 214509 (2004).
[23] J. Pascale, Phys. Rev. A **28**, 632 (1983).
[24] J. Reho, J. Higgins, C. Callegari, K. K. Lehmann, and G. Scoles, J. Chem. Phys. **113**, 9686 (2000); J. Reho *et al.*, *ibid.* **113**, 9694 (2000).
[25] M. Shapiro, J. Phys. Chem. A **110**, 8580 (2006).